Mesoscopic Phase Coherence in a Quantum Spin Fluid

Guangyong Xu, *et al.*

Science **317**, 1049 (2007);
DOI: 10.1126/science.1143831

Science (print ISSN 0036-8075; online ISSN 1095-9203) is published weekly, except the last week in December, by the American Association for the Advancement of Science, 1200 New York Avenue NW, Washington, DC 20005.

Mesoscopic Phase Coherence in a Quantum Spin Fluid

Guangyong Xu,[1,2]* C. Broholm,[1,3] Yeong-Ah Soh,[4] G. Aeppli,[5] J. F. DiTusa,[6] Ying Chen,[1,3] M. Kenzelmann,[1,3] C. D. Frost,[7] T. Ito,[8] K. Oka,[8] H. Takagi[8,9]

Mesoscopic quantum phase coherence is important because it improves the prospects for handling quantum degrees of freedom in technology. Here we show that the development of such coherence can be monitored using magnetic neutron scattering from a one-dimensional spin chain of an oxide of nickel (Y_2BaNiO_5), a quantum spin fluid in which no classical static magnetic order is present. In the cleanest samples, the quantum coherence length is 20 nanometers, which is almost an order of magnitude larger than the classical antiferromagnetic correlation length of 3 nanometers. We also demonstrate that the coherence length can be modified by static and thermally activated defects in a quantitatively predictable manner.

A wave is deemed coherent when it is perfectly periodic in space and time. Quantum-mechanical phase coherence means that the corresponding wave function is actually a coherent wave. Typically, though, classical disorder limits quantum phase coherence. The occasions where this is not the case and the quantum phase coherence length far exceeds that given by classical considerations remain a major theme of physics. The longstanding examples are superconductivity and superfluidity, in which macroscopic quantum phase coherence (*1*) has been revealed by persistent current and Josephson junction experiments (*2*, *3*). The effects of phase coherence have also been seen recently in the incompressible quantum fluid phase of two-dimensional (2D) electron gas (*4*) and in a laser-cooled Bose-Einstein condensate (*5*). Curiously, although magnetism itself is a quantum mechanical phenomenon, originating from the shell model of the atom, mesoscopic (in the sense of extending over distances in excess of 10 nm) quantum coherence in the absence of classical static order has not been explicitly demonstrated for a magnet. We show that the development of such coherence can be readily monitored with the use of magnetic neutron scattering from a 1D spin chain, in the form of an oxide of nickel, and that it is limited by static and thermally activated defects.

One of the best-known magnets that remains disordered because of quantum fluctuations is a chain of integer spins coupled antiferromagnetically (that is, favoring antiparallel alignment) to their neighbors (*6*, *7*). The two-spin correlation function $\langle \mathbf{S}_j \cdot \mathbf{S}_{j'} \rangle$, where j and j' are site indices of the spins, decays exponentially with large distances $|j - j'|$ between spins S_j and $S_{j'}$ in the chain as in a 1D liquid; whereas in a classical magnet, static correlations persist over macroscopic length scales when the system orders. Even so, theoretical work has shown that the ground state is coherent in the sense that the more complex "string" correlation function (*8*), $O(j-j') = \langle S^z_j \exp[i\pi \sum_{j<k<j'} S^z_k] S^z_{j'} \rangle$, tends to a constant (*9*) for $j - j' \to \infty$. A simple way to understand the string order is to look at the spin chain in terms of the spin-projection quantum numbers $S^z = -1$, 0, and +1 at individual sites. Correspondingly, for S = 1, the basis states are $|\pm 1\rangle$, which has clear classical analogs and can be used to build a perfect Néel state $|\ldots{-}1,{+}1,{-}1,{+}1,{-}1,{+}1\ldots\rangle$ for the chain, and $|0\rangle$, which does not. String order is carried by states where sites with $S^z = 0$ are inserted into the perfect Néel state (Fig. 1B). A good approximation to the ground-state wave function for the Heisenberg S = 1 chain is a coherent superposition of all such states with a weighting factor that decreases exponentially with the number of $|0\rangle$ sites (*10*). In general, long-range quantum coherence is believed to exist in all 1D systems with spectral gaps (*11*).

For the spin-1 chain, the lowest excited state above the ground state entails inserting a defect into the string order. The defect can propagate throughout the lattice (Fig. 1C) until it encounters another defect, and so will have a mean free path limited by either static defects, such as

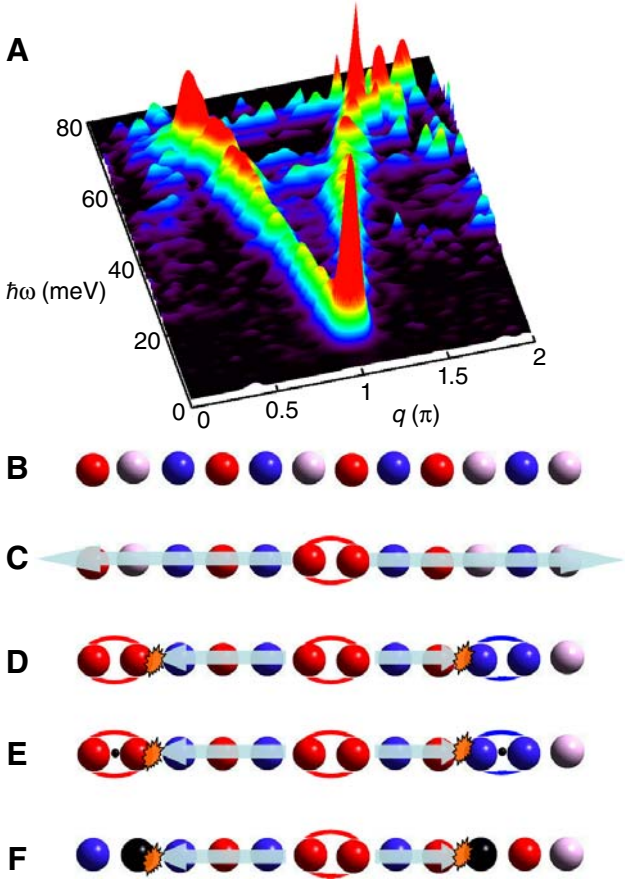

Fig. 1. (**A**) Map of the dynamic spin-correlation function multiplied by energy for the 1D spin-1 chain Y_2BaNiO_5 at low temperature (T = 10 K). (**B** to **F**) Diagrams of the string order in the spin-1 chain. The red, blue, and gray spheres represent sites with S^z of 1, –1, and 0, respectively. Chemical impurities are represented by large black spheres (Mg). (B) S = 1 chain at T = 0 and no chemical impurity. (C) One triplet wave packet propagating on the chain. (D) At $T > 0$, triplet wave packets act as thermal defects and confine each other into boxes. (E) Box confinement by Ca impurities, which introduce holes (indicated by small black spheres) into the chain and cause neighboring spins to form ferromagnetic pairs. (F) Box confinement by Mg impurities, which remove Ni spins from the chain.

[1]Department of Physics and Astronomy, The Johns Hopkins University, Baltimore, MD 21218, USA. [2]Condensed Matter Physics and Materials Sciences Department, Brookhaven National Laboratory, Upton, NY 11973, USA. [3]NIST Center for Neutron Research, National Institute of Standards and Technology (NIST), Gaithersburg, MD 20899, USA. [4]Department of Physics and Astronomy, Dartmouth College, Hanover, NH 03755, USA. [5]London Centre for Nanotechnology and Department of Physics and Astronomy, University College London, 17–19 Gordon Street, London, WC1H OAH UK. [6]Department of Physics and Astronomy, Louisiana State University, Baton Rouge, LA 70803, USA. [7]ISIS Facility, Rutherford Appleton Laboratory, Chilton, Didcot OX11 0QX, UK. [8]National Institute of Advanced Industrial Science and Technology, Tsukuba, Ibaraki 305–8562, Japan. [9]Department of Advanced Materials Science, Graduate School of Frontier Sciences, University of Tokyo, Kashiwa, Chiba 277–8561, Japan.

*To whom correspondence should be addressed. E-mail: gxu@bnl.gov

chain terminations (*12*, *13*) (Fig. 1, E and F), or other moving, thermally excited defects of the same type (Fig. 1D). Thus, the coherence of the ground state should be manifested in the mean free path of its triplet excitations. By imaging these excitations and their mean free path using inelastic neutron scattering, we can establish the perfection, or quantum coherence, of the ground state.

Neutron scattering measures the Fourier transform $S(q,\omega)$ in space and time of the magnetic correlation function $\langle \mathbf{S}_j(0) \cdot \mathbf{S}_j(t) \rangle$. The experiments were conducted on single crystals of Y_2BaNiO_5, which contain an ensemble of spin-1 chains formed by the O-Ni-O backbone of corner-linked NiO_6 octahedra (*14*, *15*). The system behaves as a quantum spin liquid because of the 1D nature of the magnetic interactions. That this liquid is not a conventional classical liquid, however, is clear from Fig. 1A, which shows the full dynamical structure factor $S(q,\omega)$, multiplied by energy transfer $\hbar\omega$, for Y_2BaNiO_5. Instead of broad overdamped excitations, which soften toward zero energy as the ordering vector ($q = \pi$ in this case) for the corresponding classical solid is approached, a gapped band of well-defined modes dominates the data. The lowest-energy mode appears at $q = \pi$, and its energy is termed the Haldane gap (*6*, *7*). Alhough $S(q,\omega)$ from chemically doped Y_2BaNiO_5 is qualitatively similar, there are important differences (fig. S1). Our paper focuses on characterizing the mean free path and energetics of the lowest-energy Haldane gap mode.

The temperature (T)–dependent equal-time spin correlation length ξ_0 is shown as open circles in Fig. 2. ξ_0 is inversely proportional to the peak width of the equal-time spin correlation function $S(q) = \sum_{jj'} \langle \mathbf{S}_j \cdot \mathbf{S}_{j'} \rangle \exp\left(iq(j-j')\right)$, which in the $T \rightarrow 0$ limit directly displays the magnetic correlations built into the ground state. $S(q)$ is the magnetic analog of the structure factor measured by x-rays for ordinary liquids. Represented by the open circles in the insets of Fig. 2, A and B, $\mathbf{S}(q)$ has a maximum at $q = \pi$, indicating that the underlying classical solid is antiferromagnetic (AFM) where each spin points in a direction opposite to that of its two nearest neighbors. The peak width, however, does not vanish even as $T \rightarrow 0$, and the correlations between spins remain liquidlike for $T \rightarrow 0$, as anticipated by Haldane (*6*, *7*) and seen experimentally in several S = 1 chain compounds (*14*, *16*–*18*). The dash-dotted line in Fig. 2 is the prediction of the quantum nonlinear σ model (*19*), which is valid only for $T < \Delta/k_B$, where Δ is the Haldane gap.

The solid circles in the inset of Fig. 2 are the magnetic structure factor measured as a function of q with the energy transfer fixed, at the Haldane gap energy for insets A and B and at 36 meV for inset C. The peak approaches a resolution-limited delta function at low temperature (inset A). Because we have tuned to the gap energy, the process probed is the creation of a triplet wave packet at rest. The intrinsic width [half width at half maximum (δq)] of this peak is therefore inversely proportional to the distance over which the triplet retains quantum phase coherence. The data show that $\delta q \approx 0.007\pi$, implying phase coherence over approximately 50 lattice units a, which is much longer than the measured correlation length for AFM order ξ_0. The experiment thus provides direct evidence for mesoscopic coherence in the spin-1 chain. The peak broadens significantly when the sample is warmed (inset B) or doped by chemical impurities (inset C), indicating that quantum coherence in this system requires low temperatures and perfect crystallinity. The two length scales obtained from the two types of q scans vary differently with T. At high T, the lengths converge to nearly the same value. In contrast, as $T \rightarrow 0$, the mean free path for the Haldane gap excitation ξ nearly diverges even while the AFM length ξ_0 approaches a finite value. The AFM length is the distance between defects in the AFM order, which at $T = 0$ is simply the typical distance between sites with $S^z = 0$. Such defects do not disrupt string order. On warming, excitations in the form of ferromagnetic neighbor pairs with S^z both equal to +1 or –1 will also appear, and these disrupt not only antiferromagnetism but the underlying string order as well. Classical (gapless) AFM chains (*20*–*22*), such as the Mn^{2+} (S = 5/2) chain compound TMMC (*20*), behave very differently from Y_2BaNiO_5 in the sense that a single distance, namely the equal-time correlation length ξ_0, sets the scale for both the static and dynamic correlations.

Detailed analysis of thermal conductivity provides estimates of the magnetic mean free path in various spin chains and ladders (*23*). The results (*24*) for Y_2BaNiO_5 differ considerably from our direct measurements in the sense that they pass through a strong peak of 15a at 100 K and rapidly decrease below that, with a value of 7a at 70 K, the lowest temperature at which there was confidence in the measurements. The discrepancy with our results is not surprising given the indirect nature of the thermal conductivity measurements as well as the fact that the lower-temperature magnetothermal properties of S = 1 chains are dominated by the effective spins of chain ends rather than the triplet excitations of the entire chain segments.

To quantify the effects of chemical impurities on quantum phase coherence, consider an excited triplet wave packet on the chain. At low temperatures, the population of such wave packets is relatively low and they can travel almost freely before encountering a physical impurity, such as a chain end caused by a chemical defect. Correspondingly, the mean free path is on average half of the spin chain length. To obtain an independent measure of the latter, we recalled specific-heat work (*25*) on Y_2BaNiO_5, which showed the residual S = 1 degrees of freedom expected for chains containing odd numbers of Ni atoms (*10*, *13*, *26*). The outcome was a Curie-like dc magnetic susceptibility C/T, which we measured for the nominally pure material using superconducting quantum interference device magnetometry. The resulting Curie constant C gives an average impurity concentration of ~1.5%, or a mean distance ℓ of ~70 lattice spacings between chain breaks, which is, within error, consistent with twice the zero-T coherence length measured in our inelastic neutron-scattering experiments. The same is true for our deliberately

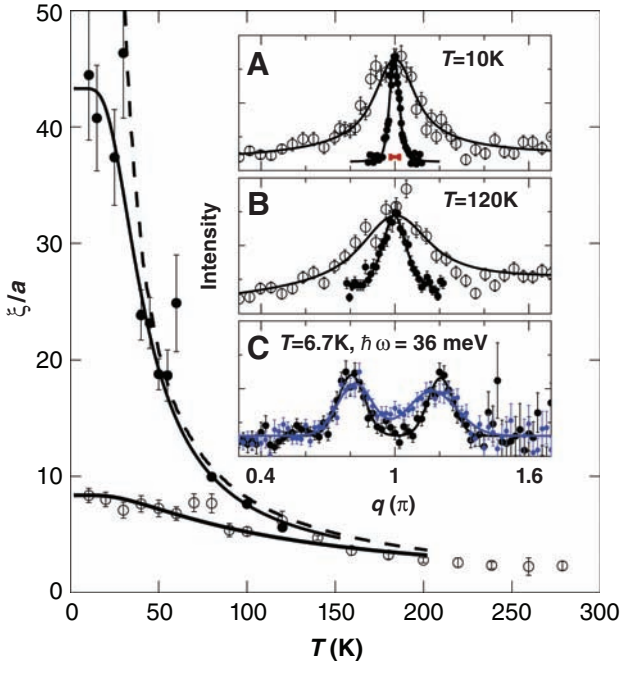

Fig. 2. Equal-time correlation length ξ_0 (open symbols) and magnetic phase coherence length ξ (solid symbols) for the 1D spin-1 chain Y_2BaNiO_5, as measured with inelastic magnetic neutron scattering (inset). Lines are theoretical results described in the text. (**A**) Low-temperature structure factor data obtained for the equal-time spin correlations ($\hbar\omega > 8$ meV) (open circles), and the bottom of the Haldane continuum at $\hbar\omega =$ 7.5 meV (solid circles, where instrument resolution is shown as the red horizontal bar) in a nominally pure sample. Fits to such data produced the main frame data points as described in the supporting online material. (**B**) Higher-temperature data in which the coherence length approaches the equal-time correlation length. (**C**) Data acquired at a fixed energy transfer (36 meV) for the nominally pure (black symbols) and Ca-doped ($Y_{2-x}Ca_xBaNiO_5$, x = 0.1) samples (blue symbols).

doped (with Ca and Mg) samples. The coherence lengths extracted from samples with nominal Ca doping of 4% and 10% ($Y_{2-x}Ca_xBaNiO_5$) and Mg doping of 4% ($Y_2BaNi_{1-x}Mg_xO_5$) were 9(1), 5(1), and 10(1) Ni-Ni spacings a, respectively, which is consistent with the scenario suggested above, for which $2\xi/a = 1/x$.

With increasing temperature and therefore triplet population, the mean free path will be limited by both thermally created defects and chain ends. In keeping with the physical picture developed above, the coherence length should approximately match half the inverse density of all (chemical and thermal) defects $\xi/a = [x + \rho(T)]^{-1}/2$. Here $\rho(T) = 3\sqrt{\frac{k_B T\Delta}{2\pi v^2}}\exp\left(-\Delta/k_B T\right)$ is the thermal triplet density (*27*) and $v = 70$ meV is the triplet velocity (*14*). The corresponding solid line in Fig. 2 shows that this model provides an excellent description of the T-dependent quantum coherence length.

Another consequence of the above picture should be a finite temperature blue shift as triplets confine each other into boxes. In other words, quantum mechanics acts not only to produce the singlet Haldane ground state and the associated gap to triplet excited states, but also gives quantum particlelike properties to the excited states, including a kinetic quantum confinement contribution. Instead of being created with energy Δ, the triplet is created with an additional kinetic energy given by the curvature of the dispersing mode shown in Fig. 1A, associated with a quasiparticle of nonzero momentum $q \sim 1/\xi$. Such a quantum contribution is found on warming as well as doping, where the quantum confinement is due to fixed boundaries. Experimentally, others have also noticed the thermally induced blue shift for Y_2BaNiO_5 (*28*) as well other Haldane systems (*17*, *29*, *30*).

Figure 3, A and B, show the temperature dependence of the mean triplet energy (Δ) and the half-width at half-maximum HWHM ($\hbar\Gamma$) of the triplet, assuming Gaussian or Lorentzian spectral functions, respectively. The measured Haldane gap (see also fig. S2) moves to higher energies on warming, which is exactly the thermal blue shift anticipated. The energy width of the triplet excitation in the $T \rightarrow 0$ limit is resolution-limited, imposing an upper bound of $\hbar\Gamma = 0.1$ meV on the excited-state relaxation rate. This means that the lifetime of the triplet is $>10^{-10}$ s, implying a quality factor for the triplet oscillations $Q = \Delta/\hbar\Gamma > 100$. This represents the largest (by an order of magnitude) bound on Q reported to date for an S = 1 chain. When we introduce excited states through warming, the HWHM increases, thus providing evidence for an increasing triplet relaxation rate, which goes hand in hand with the reductions in mean free path discussed above.

Although the quantum nonlinear σ model (*19*) provides a reasonable prediction for the spin correlation lengths, it severely overestimates the thermal blue shift (the dash-dotted line in Fig. 3A). A more successful approach exploits Monte Carlo calculations (*31*), which provide the $T = 0$ gap energy due to finite chain confinement. By using twice the coherence length ξ obtained in Fig. 2 as the size of the confinement "box" (top scale in Fig. 3A), the gap energies can be calculated and plotted as the blue solid line in Fig. 3. The agreement between experimental data and the parameter-free calculation is truly remarkable. It is also worthwhile to note that introducing chemical impurities is another approach to creating the same quantum confinement effect. Average gap energies for 4 and 10% Ca-doped and 4% Mg-doped Y_2BaNiO_5 are extracted from measurements done at base temperature and plotted as diamonds in Fig. 3A, which agree very well with the calculated gap energies based on $2\xi/a = 1/x$.

Although we have described all of our T-dependent data in terms of a very simple model whose underlying driver is thermal activation across a gap to triplet formation, it is important to realize that this model is largely phenomenological. Fortunately, there is a rigorous formulation, with similar conclusions, due to Damle and Sachdev (*27*), whose finite temperature theory is based on a semiclassical treatment of scattering between triplet excited states with a temperature-independent quadratic dispersion relation. Although this parameter-free theory does not account for the thermal blue shift, it determines the triplet lifetime and leads to the phenomenological expression for ξ in the clean limit ($x = 0$), in impressive agreement (dashed lines in Figs. 2 and 3B) with the data.

Our experiments have shown that although quantum spin chains with a gap have a finite equal-time spin correlation length, the coherence of excited states at low temperature is limited only by quenched disorder. At finite temperatures, the coherence length decreases and the excited states acquire a finite mean free path due to collisions with other excitations. Both effects are quantitatively accounted for by a semiclassical theory of triplet wave packets scattering from each other and from defects in the sample. This demonstration of mesoscopic phase coherence in a magnet adds a fifth example—the other four are superconductors, superfluids, fractional quantum Hall states, and optically confined Bose-Einstein condensates—to the list of systems in which quantum phase coherence has been demonstrated in the absence of classical order.

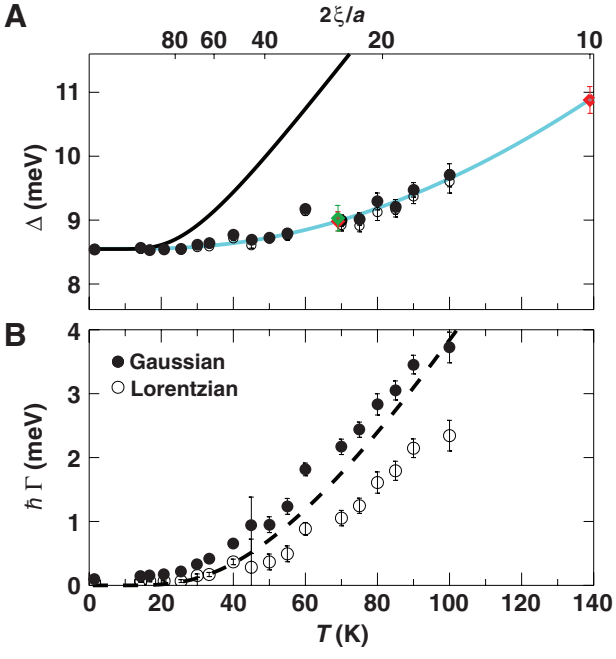

Fig. 3. (**A**) Haldane gap energy, and (**B**) half width of the excited triplet mode measured at different temperatures for Y_2BaNiO_5. The open and solid circles are results from assuming Lorentzian and Gaussian spectral functions, respectively, which the data do not distinguish. The lines in (A) are model calculations described in the text. The dashed line in (B) is a parameter-free theoretical result (*27*). The diamonds are gap energies derived from measurements at base temperature on Ca (red)– and Mg (green)–doped samples (concentration x) and placed according to $2\xi/a = 1/x$ of the top scale in (A), which indicates the effective thermal chain lengths for a pure sample (twice the coherence length from the dashed line in Fig. 2), resulting from thermal defects.

References and Notes

1. In superconductors and superfluids, phase coherence is macroscopic, whereas the microscopic coherence lengths associated with the single or paired particles participating in the condensate are finite and remain so down to zero temperature. The equal-time correlation length ξ_0 in the experiments reported here is analogous to the latter quantity.
2. B. D. Josephson, *Phys. Lett.* **1**, 2511 (1962).
3. L. B. Ioffe *et al.*, *Nature* **415**, 503 (2002).
4. M. Kellogg, J. P. Eisenstein, L. N. Pfeiffer, K. W. West, *Phys. Rev. Lett.* **93**, 036801 (2004).
5. M. R. Andrews *et al.*, *Science* **275**, 637 (1997).
6. F. D. M. Haldane, *Phys. Lett. A* **93**, 464 (1983).
7. F. D. M. Haldane, *Phys. Rev. Lett.* **50**, 1153 (1983).
8. M. den Nijs, K. Rommelse, *Phys. Rev. B* **40**, 4709 (1989).
9. U. Schollwock, Th. Jolicoeur, T. Garel, *Phys. Rev. B* **53**, 3304 (1996).
10. I. Affleck, T. Kennedy, E. H. Lieb, H. Tasaki, *Phys. Rev. Lett.* **59**, 799 (1987).
11. B. L. Altshuler, R. M. Konik, A. M. Tsvelik, *Nucl. Phys. B* **739**, 311 (2006).
12. G. Xu *et al.*, *Science* **289**, 419 (2000).
13. M. Kenzelmann *et al.*, *Phys. Rev. Lett.* **90**, 087202 (2003).
14. G. Xu *et al.*, *Phys. Rev. B* **54**, R6827 (1996).
15. Materials and methods are available as supporting material on *Science* Online.
16. W. J. L. Buyers *et al.*, *Phys. Rev. Lett.* **56**, 371 (1986).
17. J. P. Renard, M. Verdaguer, L. P. Regnault, W. A. C. Erkelens, J. Rossat-Mignod, *J. Appl. Phys.* **63**, 3538 (1988).

18. L. P. Regnault, I. A. Zaliznyak, J. P. Renard, C. Vettier, *Phys. Rev. B* **50**, 9174 (1994).
19. Th. Jolicur, O. Golinelli, *Phys. Rev. B* **50**, 9265 (1994).
20. M. T. Hutchings, G. Shirane, R. J. Birgeneau, S. L. Holt, *Phys. Rev. B* **5**, 1999 (1972).
21. J. Skalyo Jr., G. Shirane, R. J. Birgeneau, H. J. Guggenheim, *Phys. Rev. B* **2**, 4632 (1970).
22. S. Itoh, Y. Endo, K. Kakurai, H. Tanaka, *Phys. Rev. Lett.* **74**, 2375 (1995).
23. A. V. Sologubenko, T. Lorenz, H. R. Ott, A. Freimuth, *J. Low Temp. Phys.* **147**, 387 (2007).
24. K. Kordonis, A. V. Sologubenko, T. Lorenz, S.-W. Cheong, A. Freimuth, *Phys. Rev. Lett.* **97**, 115901 (2006).
25. A. P. Ramirez, S.-W. Cheong, K. L. Kaplan, *Phys. Rev. Lett.* **72**, 3108 (1994).
26. M. Yoshida *et al.*, *Phys. Rev. Lett.* **95**, 117202 (2005).
27. K. Damle, S. Sachdev, *Phys. Rev. B* **57**, 8307 (1998).
28. T. Sakaguchi, K. Kakurai, T. Yokoo, J. Akimitsu, *J. Phys. Soc. Jpn.* **65**, 3025 (1996).
29. A. Zheludev *et al.*, *Phys. Rev. B* **53**, 15004 (1996).
30. M. Kenzelmann, R. A. Cowley, W. J. L. Buyers, D. F. McMorrow, *Phys. Rev. B* **63**, 134417 (2001).
31. M. P. Nightingale, H. W. J. Blöte, *Phys. Rev. B* **33**, 659 (1986).
32. We thank K. Damle, B. Keimer, S. Sachdev, S. Shapiro, and J. M. Tranquada for helpful discussions. Work in London was supported by a Wolfson–Royal Society Research Merit Award and the Basic Technologies program of Research Councils UK. Work at Johns Hopkins University, NIST, and Louisiana State University was supported by NSF and that at Brookhaven National Laboratory was supported by the Office of Science of the U.S. Department of Energy.

Supporting Online Material
www.sciencemag.org/cgi/content/full/1143831/DC1
Materials and Methods
Figs. S1 and S2
References

16 April 2007; accepted 12 July 2007
Published online 26 July 2007;
10.1126/science.1143831
Include this information when citing this paper.

Electron-Induced Oxygen Desorption from the TiO_2(011)-2×1 Surface Leads to Self-Organized Vacancies

Olga Dulub,[1] Matthias Batzill,[2] Sergey Solovev,[3] Elena Loginova,[3] Alim Alchagirov,[1] Theodore E. Madey,[3] Ulrike Diebold[1]*

When low-energy electrons strike a titanium dioxide surface, they may cause the desorption of surface oxygen. Oxygen vacancies that result from irradiating a TiO_2(011)-2×1 surface with electrons with an energy of 300 electron volts were analyzed by scanning tunneling microscopy. The cross section for desorbing oxygen from the pristine surface was found to be 9 (±6) × 10^{-17} square centimeters, which means that the initial electronic excitation was converted into atomic motion with a probability near unity. Once an O vacancy had formed, the desorption cross sections for its nearest and next-nearest oxygen neighbors were reduced by factors of 100 and 10, respectively. This site-specific desorption probability resulted in one-dimensional arrays of oxygen vacancies.

Desorption of atoms or molecules can occur when sufficient energy is available to overcome the potential barrier that forms the surface bond. Often this process occurs through thermal routes and the barrier is overcome through vibrational energy, but electronic transitions induced by photons or particles (typically electrons or ions) can lead to rapid desorption when the atom or molecule is excited to a higher-energy configuration that is repulsive in nature. This desorption induced by electronic transitions (DIET) has important fundamental and technological applications (*1*, *2*). DIET-related phenomena must be taken into account in areas as diverse as the modification of semiconductors (*3*), the radiation damage of optical materials (*4*, *5*), nuclear waste storage, and planetary science (*6*, *7*). By using the tip of a scanning tunneling microscope (STM) as an electron source, such processes can be used for the electronic control of single-molecule dynamics (*8*–*10*).

[1]Department of Physics, Tulane University, New Orleans, LA 70118, USA. [2]Department of Physics, University of South Florida, Tampa, FL 33620, USA. [3]Department of Physics and Astronomy and Laboratory for Surface Modification, Rutgers University, Piscataway, NJ 08855, USA.

*To whom correspondence should be addressed. E-mail: diebold@tulane.edu

Central to DIET phenomena is the efficient conversion of an initial electronic excitation into the motion of an atom. One of the earliest proposed mechanisms (*11*, *12*) invokes a Frank-Condon excitation of an adsorbate to a repulsive potential energy curve; under strong excitation conditions, such excitations can also be achieved by multiple electronic transitions (DIMET) (*13*). Desorption will occur only if the electronic excitation is long-lived and the nucleus starts to move before the excitation is quenched. Understanding the basic physics that quenches such excitations is important for technical applications, for example, in processes that convert solar energy into chemical reactions or electrical energy (*14*) or in contamination of optical elements in extreme ultraviolet lithography applications (*15*).

DIET processes differ from thermal desorption in several important ways. Surface species undergoing thermal desorption are close to equilibrium in that the vibrational energy can redistribute rapidly relative to the time scale of breaking surface bonds. Thermal desorption usually involves neutral species, but the much higher energies available in DIET processes allow charged species to leave the surface and overcome attractive forces, and cascading electron transfer processes can lead to desorption of anions, cations, metastables, and ground-state neutrals. Because thermal desorption processes are near to equilibrium, the effect of a desorption event on the remaining surface neighbors is a small perturbation; rapid diffusion will delocalize and randomize vacancies created by desorption. In DIET processes that occur far from equilibrium at low temperature, a vacancy created by desorption remains localized and cannot diffuse. One might expect that such immobile DIET-produced vacancies would be randomly arrayed on the surface.

We have investigated one of the canonical materials for studying DIET processes, TiO_2, and we find highly unusual and unexpected behavior for vacancy distributions on the (2×1) termination of TiO_2(011): Electron bombardment leads to formation of vacancy clusters, one-dimensional arrays of O vacancies. Why? Although the initial probability for O^+ desorption and the formation of an O vacancy is nearly unity, the creation of a vacancy markedly decreases the desorption probability of its nearest-neighbor and next-nearest-neighbor O atoms. The surface charge that accompanies defect formation must be the factor causing desorption probabilities to change so greatly.

Self-organization can be achieved where an initial process controls subsequent events. A string of such interrelated events can then lead to pattern formation. The unexpectedly high alteration of the desorption probability upon formation of an O vacancy is an example of this phenomenon; the initial desorption event is responsible for the self-organization of subsequent defects. This process should apply generally to DIET processes. Consequently, the formation of well-defined O-vacancy patterns must be taken into consideration in the radiation damage of insulating surfaces and can be used to enhance the chemical reactivity of DIET-modified surfaces.

We have investigated the effects of electron irradiation on TiO_2 not only because it has been a model system for DIET processes, but because it is a very promising material for solar energy conversion; it is also the prototypical material for fundamental studies of metal oxide surface reactivity (*16*, *17*). Its chemical, electronic, and optical properties depend strongly on the presence of steps, vacancies, and other surface defects